J. Fluid Mech. (2003), *vol.* 486, *pp.* 239–259.
DOI: 10.1017/S0022112003004634 Printed in the United Kingdom

Dynamics of a dry spot

By S. G. BANKOFF[1], M. F. G. JOHNSON[1], M. J. MIKSIS[2], R. A. SCHLUTER[3] AND P. G. LOPEZ[4]

[1]Department of Chemical Engineering, Northwestern University, Evanston, IL 60208, USA

[2]Department of Engineering Sciences and Applied Mathematics, Northwestern University, Evanston, IL 60208, USA

[3]Department of Physics and Astronomy, Northwestern University, Evanston, IL 60208, USA

[4]CICESE, Division de Física Aplicada, Ensenada, BC 22860, Mexico

(Received 4 September 2001 and in revised form 3 February 2003)

Experimental results are presented for the motion of a dry spot in a thin viscous film on a horizontal surface. These include global and spatial measurements of dry spot diameter, front velocities, static and dynamic contact angle, and the shape of the liquid–solid interface. Data are presented as a function of initial fluid depth for both an advancing fluid front of a collapsing dry spot and a receding fluid front of an opening dry spot. Results for both cases show that the final or static hole diameter increases as the initial fluid depth decreases. Also, insight is obtained into the relationship between the contact angle and the velocity for both advancing and receding fluid fronts. The experimental results are compared to a lubrication model, and good agreement is obtained.

1. Introduction

The aim of most coating processes is to produce a uniform film on the solid. Owing to a number of constraints on the final product, e.g. a very thin coating film, the process can have a number of instabilities associated with it. Included among these are an instability at the leading edge of the coating film and the formation of air pockets, or dry spots, within the film itself. Under certain circumstances, these dry spots can simply disappear, whereas in other cases they do not and could remain in the final product as a defect of the process. Our aim here will be to present a basic experimental study of the dynamics of a dry spot. We will be interested in how the physical properties of the film affect its dynamics and resulting equilibrium solutions. Our experimental results compare very well with a theoretical model of the dynamics of a dry spot.

The isothermal problem of the growth and collapse of a dry spot in a thin liquid film is a classical problem. Equilibrium solutions for the profiles of axisymmetric systems have been well-documented since the early works of Lamb (1916) and Padday (1971). In a theoretical and experimental study of axisymmetric holes in liquid films, Taylor & Michael (1973) showed that when the film sheet extends to infinity, an equilibrium solution which is energetically unstable exists for a film of thickness less than some critical value. The results of their experimental investigation of holes in mercury on glass suggest that the equilibrium position serves to distinguish between holes which open and those which close. Contrary to these results, their experiments on holes in water standing on paraffin wax gave no sharp distinction between opening and closing holes. In addition, they found that there was a wide range of holes which

could remain stationary. They concluded the reason for this behaviour was related to the contact angle at the liquid/gas/solid intersection. Experimental results similar to these are also observed here.

Sharma & Ruckenstein (1990) showed that, theoretically, for a given contact angle in a finite domain, two equilibrium holes of different radii are feasible. Using an energy argument, they showed that the dry spot with the larger radius is unconditionally stable while the one with the smaller radius is unstable. The implication of this calculation is that a dry spot larger than the unstable one will open while smaller holes will close. These could be considered as a generalization of the results of Taylor & Michael (1973) to finite domains. Moriarty & Schwartz (1993) considered the evolution of an axisymmetric dry spot in a thin liquid film on a finite domain in the lubrication limit. The contact line motion at the edge of the dry spot was taken into account in their numerical solution. Numerical slip was used at the contact line to account for the singularity there. They found that a film with a dry spot having an initial radius slightly larger than the corresponding unstable static solution, but with a higher surface energy, can actually close instead of open, as expected from the static studies. Using an asymptotic analysis, equilibrium holes in an unbounded domain have been studied by Wilson & Duffy (1996).

Diez *et al.* (1992) studied closing dry spots theoretically and experimentally in their study of the axisymmetric flow of a very viscous fluid toward a central orifice. They considered a region where there was a balance between gravity and viscous forces. A similarity solution was constructed and shown to compare well with the experimental results on closing dry spots after the radius of the dry spot was sufficiently small compared to its initial radius. The experiments and theory were done in a limit where surface tension effects were assumed to be small. Experimental work has also been done by Redon, Brochard Wyart & Rondelez (1991). They considered very thin films ($\sim 30\,\mu$m) in contrast to the present work (~ 2 mm). They found that for these very thin films an annular ring is formed which grows in width as the hole opens, but the rest of the film remains static. This is quite different from the work done here.

A theoretical study of the dynamics of dry spots in the thin-film limit was performed by Lopez, Miksis & Bankoff (2001). As did Moriarty & Schwartz (1993), they studied dry spots in a finite domain, but in this study Lopez *et al.* (2001) modelled the motion of the contact line by assuming a contact angle–slip velocity relation and a Navier slip law along the solid interface. They investigated the linear stability of the allowable equilibrium solutions and showed that as the size of the dry spot increased, the equilibrium solutions for the liquid films become unstable to non-axisymmetric disturbances. They also presented a numerical investigation of the nonlinear evolution equation showing how asymmetric disturbances can develop. Surface tension effects occur at leading order in their model. This model will be compared with experimental results found here, and good agreement will be shown.

2. Experimental facility

The facility was designed to accommodate two basic components of the system: a fluid experiment and an imaging system. The fluid experiment consists of a brass plate with an aluminium ring mounted on the surface to contain the experimental fluid (figure 1). Both the ring and the plate are painted black for the imaging system. The painted surfaces are polished to smooth the surface roughness of the paint.

A support bar over the pool of fluid supports a copper capillary tube which is positioned such that it blows a hole in the fluid in the centre of the pool. This method was previously used by Taylor & Michael (1973) for water on a wax surface.

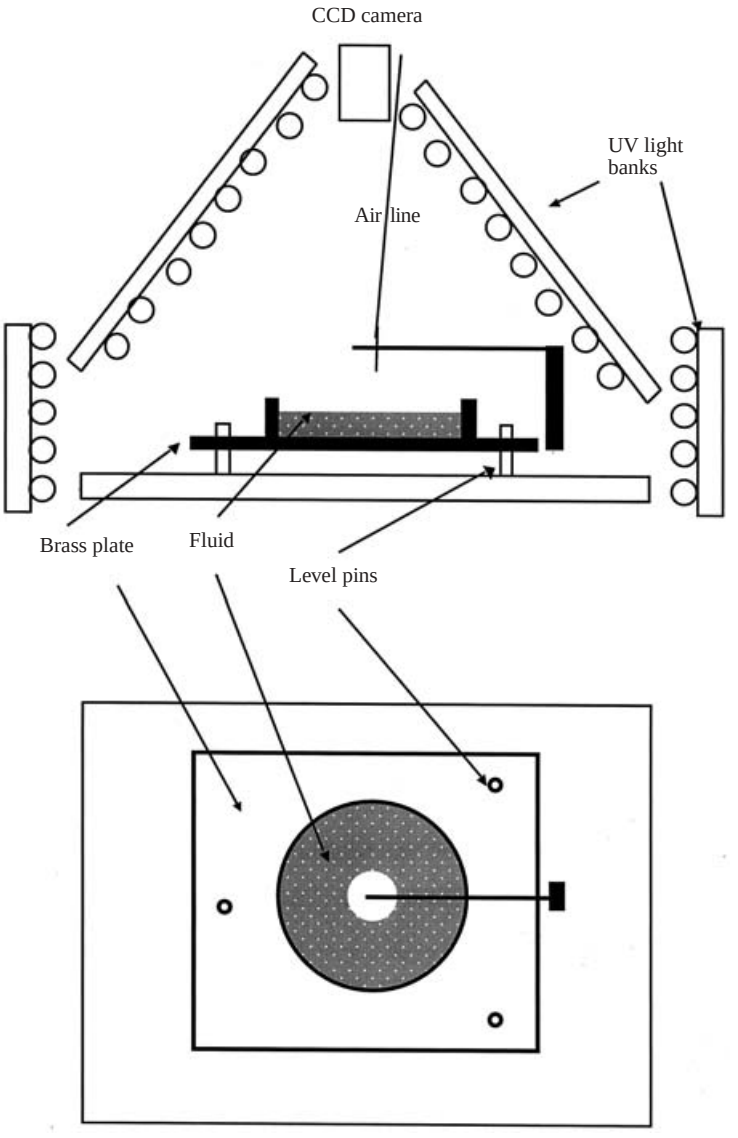

FIGURE 1. Forward and overhead view of the experimental facility.

The imaging system components are four banks of ultraviolet lights positioned along two sides of the plate and a CCD camera mounted overhead. The camera records the fluorescent intensity of the fluid when exposed to the UV lights as detailed below.

2.1. *Fluorescent imaging method*

The imaging method detailed by Johnson, Schluter & Bankoff (1997) (see also Johnson *et al.* 1999) is applied to the dry spot experiments for the measurement of fluid depth. A dye (rhodamine) has been added to the fluid mixtures such that the fluid fluoresces when exposed to the UV lights. The fluorescence level emitted by the fluid is recorded and has been shown to be convertible to a fluid depth by use of a calibration curve (Johnson 1997; Johnson *et al.* 1997). This method has a variation of approximately

Fluid	Density (± 5 kg m^{-3})	Weight (%) Glycerin ($\pm 2\%$)	Kinematic viscosity ($\pm 10^{-6}$ m^2 s^{-1})	Surface tension (± 0.002 kg s^{-2})
A	1225	87	6.46×10^{-4}	0.066
B	1087	36	3.38×10^{-6}	0.070
C	1209	80	5.36×10^{-5}	0.066

TABLE 1. Fluid properties of experimental fluids at 21°C.

± 0.02 mm, due mainly to variations of the recorded fluorescent values using the imaging software. One modification of this method for use with this work has been the positioning of the UV light to minimize the amount of additional light capture at the fluid front. Johnson *et al.* (1997) showed that this additional capture can obscure the fluid depth values used for measuring the contact angle. Pixel numbers were converted to lengths by recording an image of known length and counting the number of pixel points corresponding to this length.

2.2. *Fluid properties*

The dry spots are formed using three experimental fluids. The three fluids are labelled A, B and C, differentiated by the amount of water added to the glycerin. The properties of these fluids are given in table 1.

2.3. *Experimental method*

Initial experiments using a thin layer of fluid on the painted surface were unsuccessful because the air line would not cause the fluid to break from the surface. When the air jet was turned on, the bulk of the fluid was pushed toward the wall of the containment ring, but a thin layer remained on the plate surface. This thin layer prevented the formation of a static dry spot for all initial fluid depths. In this case, the advancing fluid front of the collapsing annular ring of fluid perfectly wetted the thin layer of the same fluid and thus all 'dry' spots would collapse completely.

In order to obtain a dry spot, the surface of the horizontal plate had to be modified. The desired wettability of the fluid and surface was achieved by applying a very thin layer of silicone oil to the painted surface. This film was allowed to soak partially into the surface and was wiped several times to remove any excess. Now, when the air jet was turned on, the thin layer of fluid was not observed, to the accuracy of our measurements.

The dry spot experiments are divided into three categories: a completely collapsing dry spot a static diameter dry spot, and an opening dry spot. All dry spots were initiated using the same method. The air hose was turned on and the air pressure adjusted to blow a hole of the desired initial diameter. An example of a hole being blown in given in figure 2. Care was taken not to blow too large a hole as this would cause the fluid to overflow the containment ring. The figure shows that the air hose can cause small waves or disturbances to form along the front of the dry spot. Fluid depth profiles show these waves to be small compared to the depth of the fluid and to disappear rapidly (within a few seconds) after the air is turned off. The air pressure is released to allow the dry spot to close, either completely or to a static diameter. The opening dry spots are formed by using a small puff of air from the air hose which is sufficient to just break the surface of the fluid. As soon as the surface is broken, the air pressure is released while the dry spot increases in diameter.

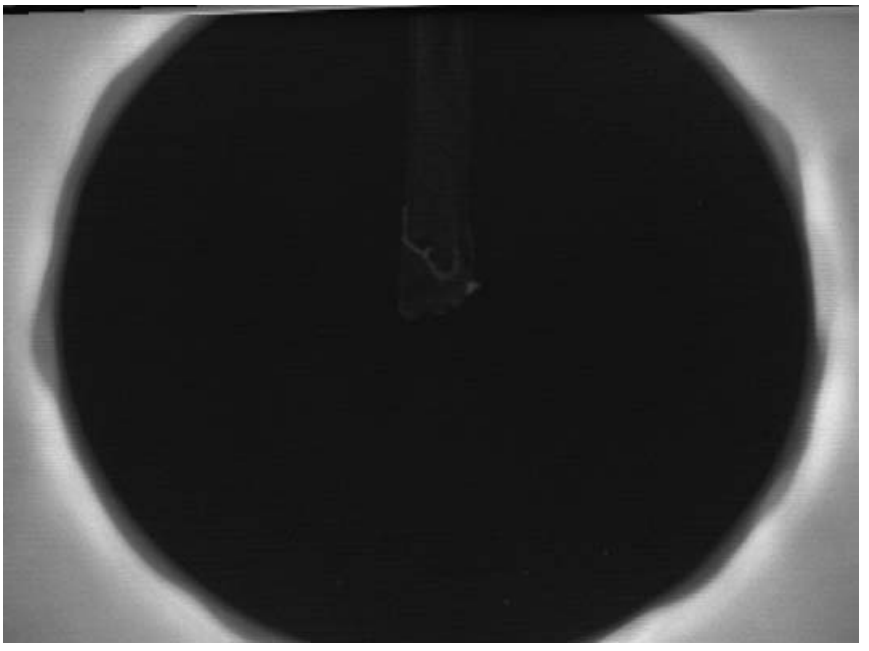

FIGURE 2. Image of an approximately 140 mm dry spot being blown on a thin layer of fluid A.

3. Lubrication model

Lopez *et al.* (2001) derived a model to study the dynamics of a dry spot in the lubrication limit. Surface tension effects entered at leading order in their model. The model assumed a cubic relation between the contact angle and the slip-velocity at the edge of the dry spot. In addition, to relax the non-integrable stress singularity at the contact line, they allowed for a Navier-slip relation along the liquid/solid interface. In their study of the dynamics of dry spots, they showed that, depending on the properties of the fluid, it was possible for non-axisymmetric modes to be the most unstable modes of motion. In addition, in the limit of small mobility, they developed a quasi-steady model of the motion of the dry spot (see Greenspan (1978) for a similar analysis). The advantage of the quasi-steady limit is that the slip coefficient from the Navier-slip law does not enter into the model at leading order and the nonlinear evolution equation for the film thickness reduces to an ordinary differential equation with time as a parameter. Lopez *et al.* (2001) examined under what conditions the quasi-steady model can be expected to give reasonable results, e.g. small mobility. Here, we will compare our experimental results against the predictions of the quasi-steady model.

We will only consider the axisymmetric version of the quasi-steady model. Let (r, z) be cylindrical coordinates. The equation for the film thickness $z = h(r, t)$ as a function of time t is

$$\sigma\left(\frac{\partial^2 h}{\partial r^2} + \frac{1}{r}\frac{\partial h}{\partial r}\right) - \rho g h = F(t), \tag{3.1}$$

in the domain $a(t) < r < L$. Here, $r = a(t)$ is the radius of the dry spot and $r = L$ is the radius of the container bounding the liquid film. Equation (3.1) is to be solved

with the boundary conditions

$$h = 0 \tag{3.2}$$

and

$$\frac{\mathrm{d}a}{\mathrm{d}t} = \frac{\sigma\omega}{2\mu}\left[\theta_s^3 - \left(\frac{\partial h}{\partial r}\right)^3\right] \tag{3.3}$$

at the boundary of the dry spot, $r = a(t)$, and

$$\frac{\partial h}{\partial r} = 0 \tag{3.4}$$

at the boundary of the container, $r = L$. The function $F(t)$ must be determined as part of the solution of the problem. This is done by the additional constraint that the volume V_0 remains constant in time

$$\int_{a(t)}^{l} rh(r, t)\,\mathrm{d}r = V_0. \tag{3.5}$$

In the above, σ is the surface tension of the liquid interface, ρ is the liquid density, g is the acceleration due to gravity, μ is the viscosity, θ_s is the static contact angle, and ω is the constant mobility of the contact line. Equations (3.1)–(3.4) are the quasi-steady model for the motion of a dry spot studied by Lopez *et al.* (2001). Solutions will also be presented here and compared to the experimental results. Generalizations and the derivation of the above model can be found in Lopez *et al.* (2001).

Finally, we should note that there is another advantage of using the quasi-steady model. By introducing a dimensionless time based on some observable time from the experiment (e.g. the total observation time) the parameter ω scales out of the problem. Hence, comparison between theory and experiment can be done without specifying this parameter.

4. Results

Results are given in the form of flow images, fluid depth profiles, static and dynamic hole diameter values, fluid front velocities and face angles. The independent experimental parameters are the fluid properties (density, surface tension and viscosity), the initial depth of the film and the diameter of the containment ring. Most of the data presented here are for a containment ring with an inner diameter of 235 mm. Data for the dry spots are divided into three categories: a closing dry spot which completely collapses; a closing dry spot which stops at a static diameter; and an opening dry spot, which also stops at a static diameter.

4.1. *Closing dry spots*

Both types of closing dry spots (full collapse and static) were visually similar. Figure 3 shows a time series of images for a fully closing dry spot bounded by fluid A. The first image is started just after the air line has been shut off. Note that the surface waves that are caused by the blown air (see figure 2), disappear within 1 s and appear not to have adverse effects on the dynamics of flow. The figure shows the dry spot collapsing symmetrically and maintaining a circular shape. This axisymmetric collapse was also observed for closing dry spots when a similar experiment was performed using the other fluids. When a closing dry spot approached a static diameter instead of completely closing, it usually maintained a circular shape during its evolution, but not as symmetric as the fully collapsing cases. The deviation was slight, but more

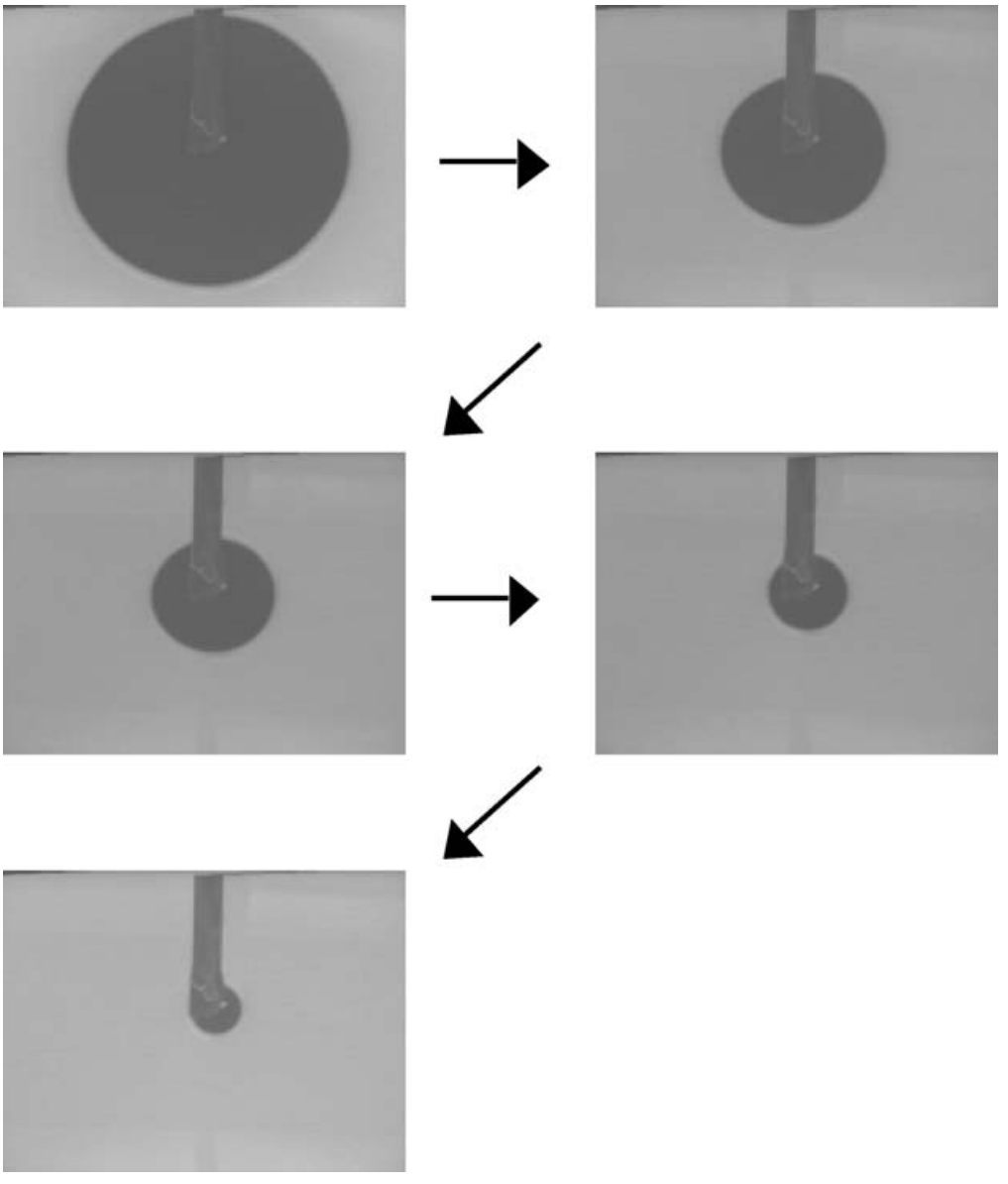

FIGURE 3. Full collapse of an initially blown dry spot. The last image shows the dry spot just before its view is obscured by the support rod for the air line. The images were taken at 1 s intervals using fluid A.

evident as the dry spot approached its final static shape. Also, static dry spots were less symmetric for the less viscous fluids (fluids B and C).

Fluid depth profiles and the shape of the fluid front as a function of time are given in figure 4 for a collapsing dry spot. The profiles are taken across the diameter of the dry spot and into the body of the film. The first profile is taken with the air line still on and is shown in the figure as the profile with the highest peaks at the farthest right and left of the figure. Each successive profile is taken after the air line is shut off and at 1 s intervals. The profiles show that the hump formed by pushing the film back with the air pressure from the air line disappears within 2–4 s. Also the

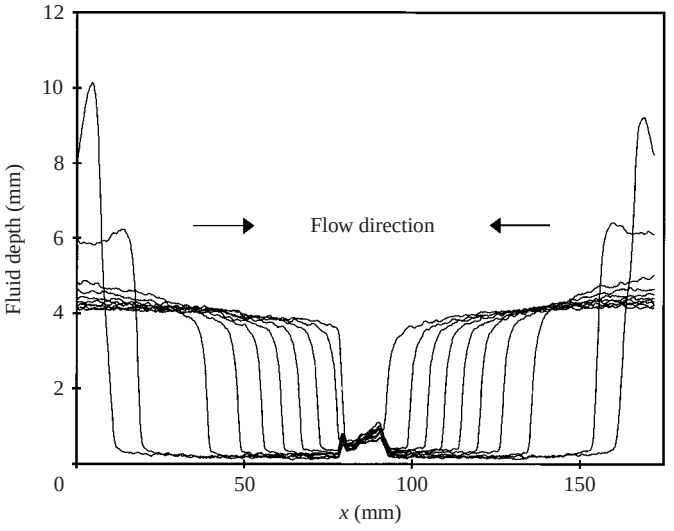

FIGURE 4. Collapse of a dry spot in a thin film of fluid A with an initial film depth $H_0 = 4.1$ mm. The plots are at 2 s intervals.

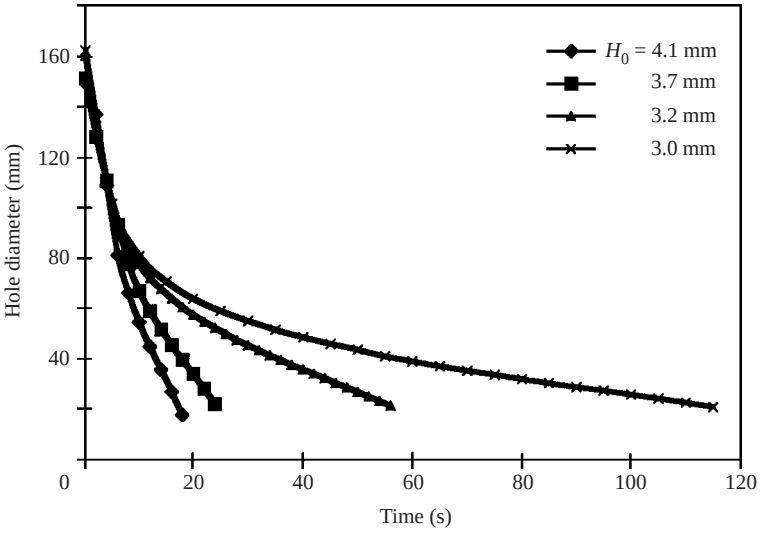

FIGURE 5. Hole diameter (mm) of a closing dry spot as a function of time (s) for varying fluid depths. Experimental fluid is fluid A.

spacing of the profiles shows that the dry spot collapses at an initially higher rate and steadily slows down as the dry spot diameter decreases. This is illustrated in figure 5 by plotting the hole diameter as a function of time. In figure 5 we plot the data points at 2 s intervals (5 s intervals for the $H_0 = 4.1$ mm case). Figure 5 shows the decrease in hole diameter as a function of time for fluid A at several different initial film depths. In all these cases, the initial fluid depth was chosen sufficiently large such that the film completely collapses. The initial hole diameters differ slightly because of the difficulty in adjusting the air flow on these scales, but the differences are not significant to the conclusions drawn below. Besides the change in hole diameter over time, the figure

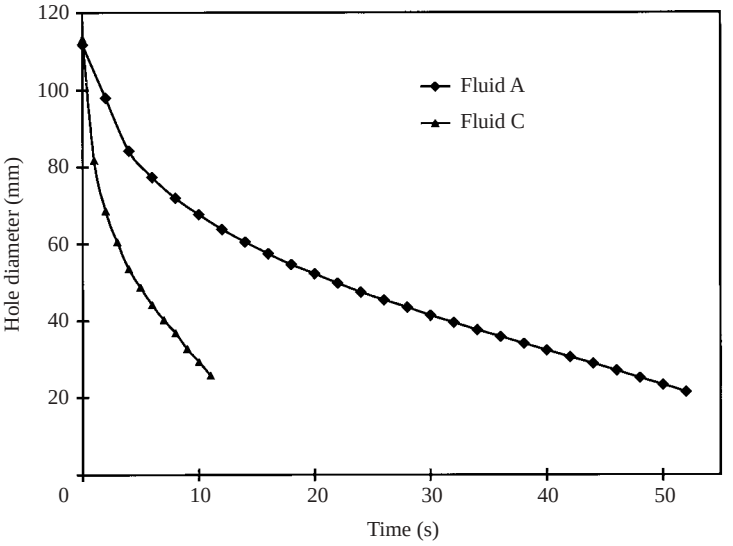

FIGURE 6. Hole diameter as a function of time for fully closing dry spots. Fluids A and C had the same initial fluid depth, $H_0 = 3.2$ mm.

also shows that the thicker the initial film, the faster the dry spot closes completely. Data were no longer collected once the hole diameter was close to the diameter of the air line support rod. Nevertheless we were able visually to estimate the time for the dry spot to collapse, t_c. For the initial film thickness $H_0 = 3.0$, 3.2, 3.7 and 4.1 mm we determined that $t_c = 137.5$, 65, 23 and 20 s, respectively. Notice that these values of t_c imply a significant change in the behavior of the curves near the collapse time. In particular, for very small hole diameters, there is a rapid rise in velocity as the hole closes. This was observed visually, and it was also noticed that a slight splash and/or trapping of an air bubble was possible during the collapse. If the hole is not too small, gravitational and viscous forces can balance in this thin film. This is the case studied by Diez *et al.* (1992). In this limit, a similarity solution can be obtained, stating that the hole radius $a(t)$ is proportional to $(t_c - t)^{\delta}$, where δ is approximately 0.76. If this is true, we can expect a very rapid decrease in the radius near the critical time for collapse. As discussed below, our results are consistent with this. For smaller dry spot radii, inertial forces are expected to become important. Because of the location of the air line, we cannot make any conclusions about this behaviour, but it can be expected that during this final stage of collapse the inertial forces should come into balance with the surface tension forces, and a similarity solution of the form discussed by Keller & Miksis (1983), i.e. $a \propto t^{2/3}$, might be expected. Additional discussion of the dynamics of small dry spots can be found in Lopez *et al.* (2001) where a relation in the quasi-steady limit (no inertial terms) between the closing time and the radius is obtained. In particular, their quasi-steady result implies that a power law might not be suitable for small radii.

Similar experiments showed the same basic trend during the collapse of a dry spot for fluids B and C. This is illustrated in figure 6 where we compare the diameter of a collapsing dry spot as a function of time for fluids A and C, which have the same initial depth of 3.2 mm. We see that the more viscous fluid (A) closed at a significantly slower rate than the less viscous fluid (C). This is the expected situation since the larger the viscosity, the larger the viscous stress in the flow field, and hence

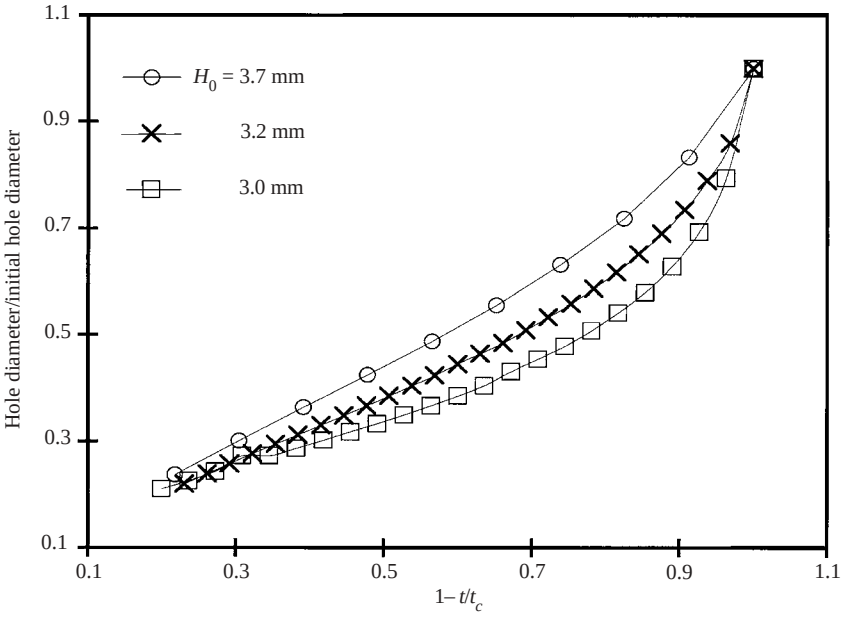

FIGURE 7. Plot of normalized hole diameter as a function of non-dimensional time. t_c is the estimated time it takes for the hole to collapse.

the slower the flow. We should note that although the hole diameters are initially the same, the initial blown profile is different owing to the different physical properties (e.g. viscosity) of the liquids.

In figure 7, we plot the fully closing hole or dry spot diameter data for fluid A in a format similar to that of Diez *et al.* (1992). They collected data for a fully closing hole of silicone oil on Perspex, using a circular dam to create an initial dry spot. Here, we have plotted the hole diameter (normalized by the initial hole diameter) versus $1 - t/t_c$. Three different initial film depths are shown and we see that these scaled results fall on very similar curves. The shapes of the curves for the data of Diez *et al.* (1992) are basically the same as for our data (figure 7), but they plot on a logarithmic scale, so that differences in the data are difficult to observe. Our range of data is slightly different as we are unable to record the last few seconds before the final closure of the hole because the air line support bar is in the view of the camera. Also, their data start with a much smaller initial hole, and much further from the containment ring. The range of our data which corresponds to their data would be for values of the non-dimensional time of less than 0.6. What is important to observe here is that although there is some qualitative agreement in the trend of the data in these units, the initial dynamics appears to differ quantitatively for each of the runs, but as the hole closes, the data appear to collapse onto a single curve.

Diez *et al.* (1992) compared their data to a model derived in the lubrication limit and found good agreement. In their theoretical analysis, surface tension was neglected and they were able to obtain a similarity solution. They argued that neglecting surface tension was a reasonable approximation since the oil–air surface tension was less than the critical surface tension for complete wetting (see e.g. de Gennes 1985). As noted in § 2.3, our surface was pre-wetted with a layer of silicone oil, which allowed dry spots to form with finite contact angles. Hence, this argument does not apply for our situation. Rather, we should look at the ratio of the characteristic length derived

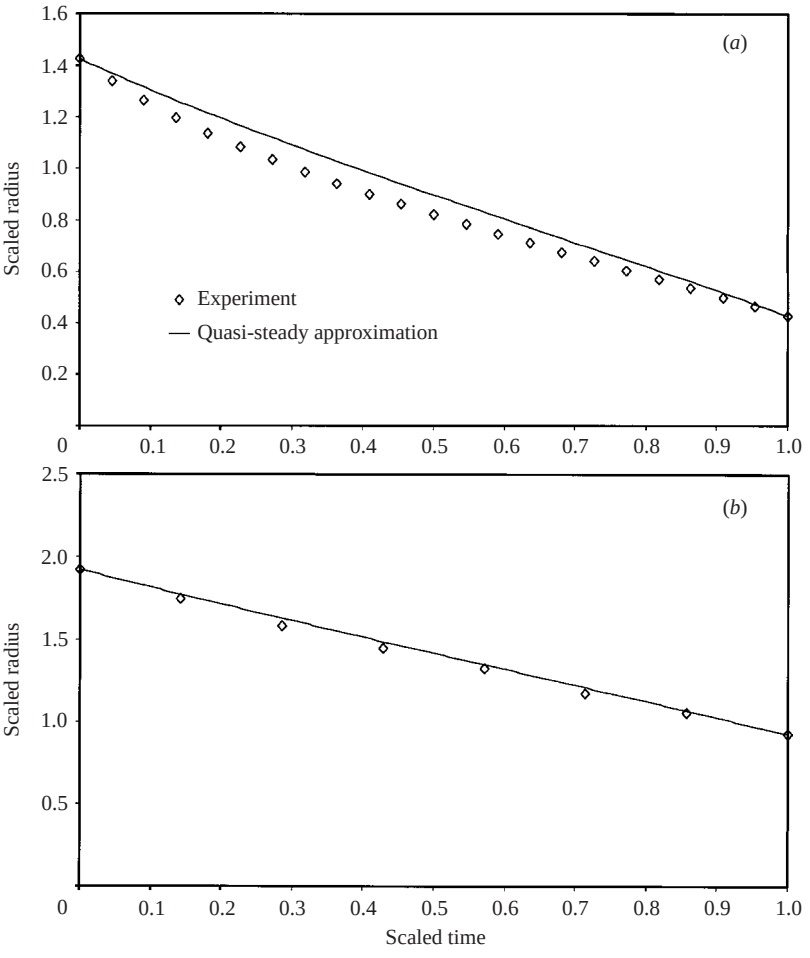

FIGURE 8. Closing dry spot. Scaled radius *vs.* scaled time. The experimental data are for (*a*) fluid A and (*b*) fluid at $h_0 = 3.2$ mm. Also, the quasi-steady model of Lopez *et al.* (2001) is plotted.

from the surface forces, to the characteristic thickness H_0 of the film, $(\sigma/\rho g)^{1/2}/H_0$. Using the data in table 1 for fluid A, and setting $H_0 = 3.0$ mm, we find this ratio to be about 0.75. The implication of this is that surface tension forces should be significant. The ratio of the film thickness to the length scale in the plane (e.g. hole diameter) is small. Hence, lubrication theory, as used in Diez *et al.* (1992), is also expected to be applicable, but surface tension forces should be included in the model. As discussed in § 3, such a model was developed by Lopez *et al.* (2001) and we will compare it to the data here. As noted above, near hole closure, the data appear to begin to collapse onto a single curve in figure 7. At this time, the velocity of the dry spot boundary becomes large, and this effect may dominate over surface-tension effects, implying that a similarity solution may become valid in this regime. We find reasonable agreement between the closure rate during the later stage of collapse of the data in figure 7 and the similarity solution of Diez *et al.* (1992), i.e. $a \propto (t_c - t)^{\delta}$, in that we find δ close to the value 0.76.

In figure 8, the results of the quasi-steady model, equations (3.1)–(3.4), are plotted along with the experimental data from figure 6. A scaled radius is plotted as a function

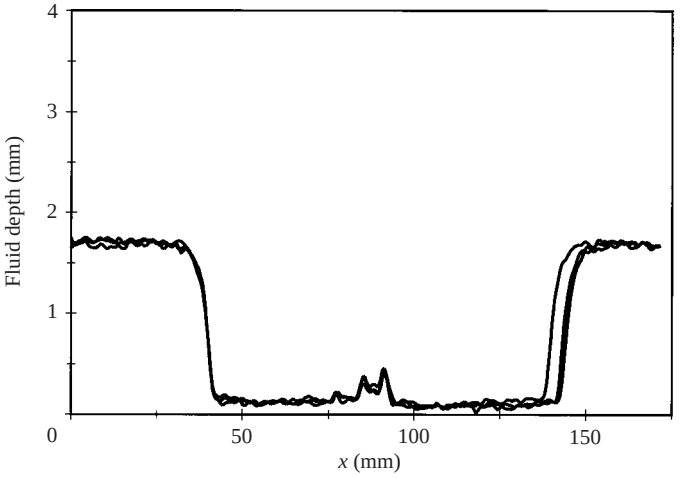

FIGURE 9. Plot of the shape and diameter of three static dry spots formed for the same initial depth and fluid.

of a scaled time. The scaled radius is equal to the dimensional radius divided by the difference between the initial radius and the final observed radius. The scaled time is equal to the dimensional time divided by the final time of observation. The physical parameters of the dry spot were taken from the experimental data. Note that the initial and final dry spot scaled radius is the same for both experiment and theory, because the initial data are the same, while the final radius is forced by selecting the static contact angle in the quasi-steady model. The resulting static angle of about 50° is consistent with the experimentally observed angles. Given these value of the parameters, we find in figure 8 very good agreement during the closing of the dry spot. These results imply that the quasi-steady model, which includes the effects of surface tension, can give reasonable predictions for the evolution of closing dry spots.

4.2. *Static dry spots*

As the initial depth of the thin film was decreased, the closing dry spots did not completely close, but reached a static shape and diameter. Figure 9 shows the final static shape for a dry spot of fluid B. The three profiles are the static shape of three successive runs for the same initial depth. The plots show the precision of the static diameter to be quite good. Generally, we observed less than a 5% variation in the static diameter for closing dry spots.

The effect of changing the initial depth of the static hole diameter is given in figure 10. The same trend of decreasing hole diameter with increasing initial depth was observed for different experimental fluids. The data sets exhibit an identical shape and are simply offset. The change in hole diameter appears to be a weakly nonlinear function of the initial depth, with about a 40% increase in depth resulting in a 55% decrease in static diameter. The behaviour of the hole diameter with initial depth seems reasonable since the final static shape is due to a balance of capillary and gravity forces along with a contact angle condition. As more fluid is added (i.e. a larger initial depth) this balance is satisfied for smaller hole diameters.

Another independent parameter which could affect the static diameter is the size of the initially blown hole. This was tested and the results are given in figure 11. The test was conducted by blowing a small hole into a film of fluid and then shutting off the air line. Initially blown holes had to be of a diameter greater than about 20 mm.

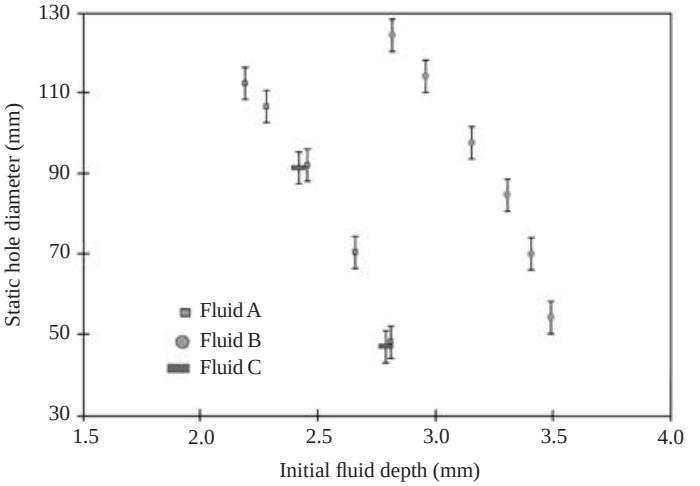

FIGURE 10. Static hole diameter as a function of initial fluid depth for closing dry spots.

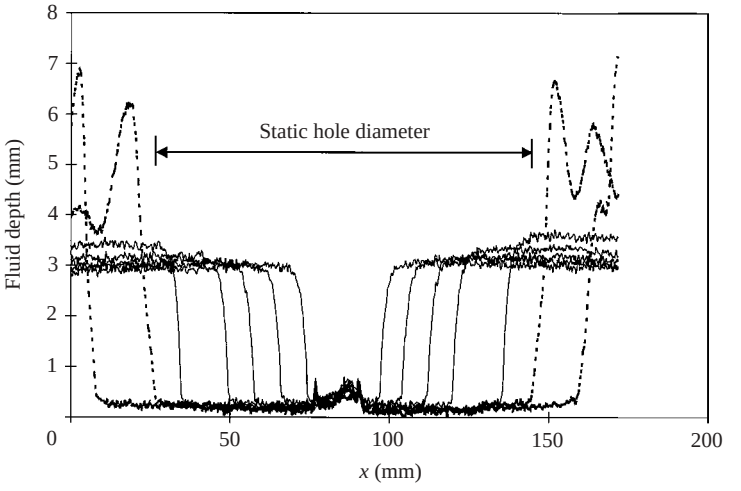

FIGURE 11. Static diameter and shape of closing dry spots blown to different initial diameters. Only spots (dotted lines in the figure) blown to a diameter larger than the static diameter labelled in the figure collapse. The dry spots of smaller diameter remained at the initial blown diameter.

Otherwise, the hole would close back to a continuous film. After sufficient time was given to record any changes in the hole diameter, a larger hole was blown and the procedure repeated. The figure shows that for holes blown for a diameter smaller than the static hole diameter (as labelled in figure 11), the dry spot experienced no detectable movement and remained at the blown diameter. However, when the blown hole diameter was greater than the static value, the dry spot would collapse to the static hole diameter. In addition, different blown large hole diameters would collapse to the same static hole diameter. We should note that the 20 mm critical blown hole diameter for complete closing can only be expected for the situations studied here and in general this critical diameter should depend on the film depth and the other parameters of the problem.

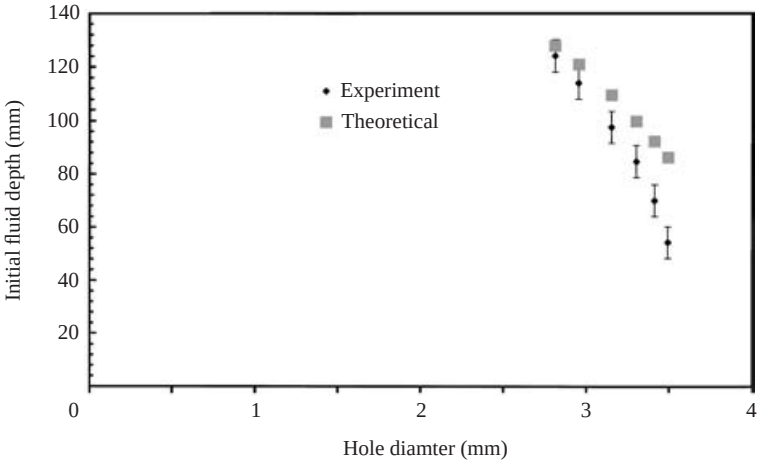

FIGURE 12. Experimental data for fluid B from figure 10 and theoretical prediction of the static dry spot diameters from Lopez *et al.* (2001).

It is interesting to ask how well the lubrication model of Lopez *et al.* (2001) compares with the experimental results for static dry spots. Recall that the theory presented in Lopez *et al.* (2001) predicts that two static profiles are possible in a container of finite size, with the profile of the larger-diameter dry spot being linearly stable. The diameter of this stable dry spot is a function of the initial film thickness (which is determined by the initial volume) and the static contact angle. The latter can be measured for each of the static profiles. In figure 12, the data from figure 10 for the fluid B case are replotted along with predictions of the lubrication model of Lopez *et al.* (2001) for the static diameter of the dry spot. Here we see about a 5% agreement between theory and experiment for the thinnest film, but as the film depth increases, the error increases to about 60% for the 3.5 mm film. We note that the results are very sensitive to errors in the estimate of the contact angle.

4.3. *Opening dry spots*

Opening dry spots were studied, paralleling our closing dry spot experiments. Opening holes were only achieved with fluids B and C. Fluid A (glycerin) never gave an opening dry spot. An example of an opening dry spot using fluid B is given in figure 13. Here we see that besides the direction of motion, the opening holes were noticeably less symmetric than the closing holes. This observation was true for both fluids B and C. Figure 14 gives the fluid depth profiles taken from the images in figure 13. The figure shows that after the thin film was broken by the puff of air, the hole diameter increased with time and the depth of the fluid behind the dry spot increased in response to this change. For the thin film in figures 13 and 14, with an initial thickness $H_0 = 1.7$ mm, the fluid film always opened, regardless of the blown hole diameter, once the air jet broke the fluid. We observed that the rate of change of the diameter was initially large and slowed as the dry spot approached its static size. The same trend was observed for a closing dry spot. The opening dry spots also followed the same trend as the closing hole for hole diameter as a function of time.

Figure 15 shows the same behaviour as figure 10, in that a smaller initial depth results in a larger static diameter. This is also shown in figure 16 which compares the static hole diameter for both the opening and closing cases for fluid B. Films of greater initial depth than 3.5 mm closed fully. Values for an initial depth between the

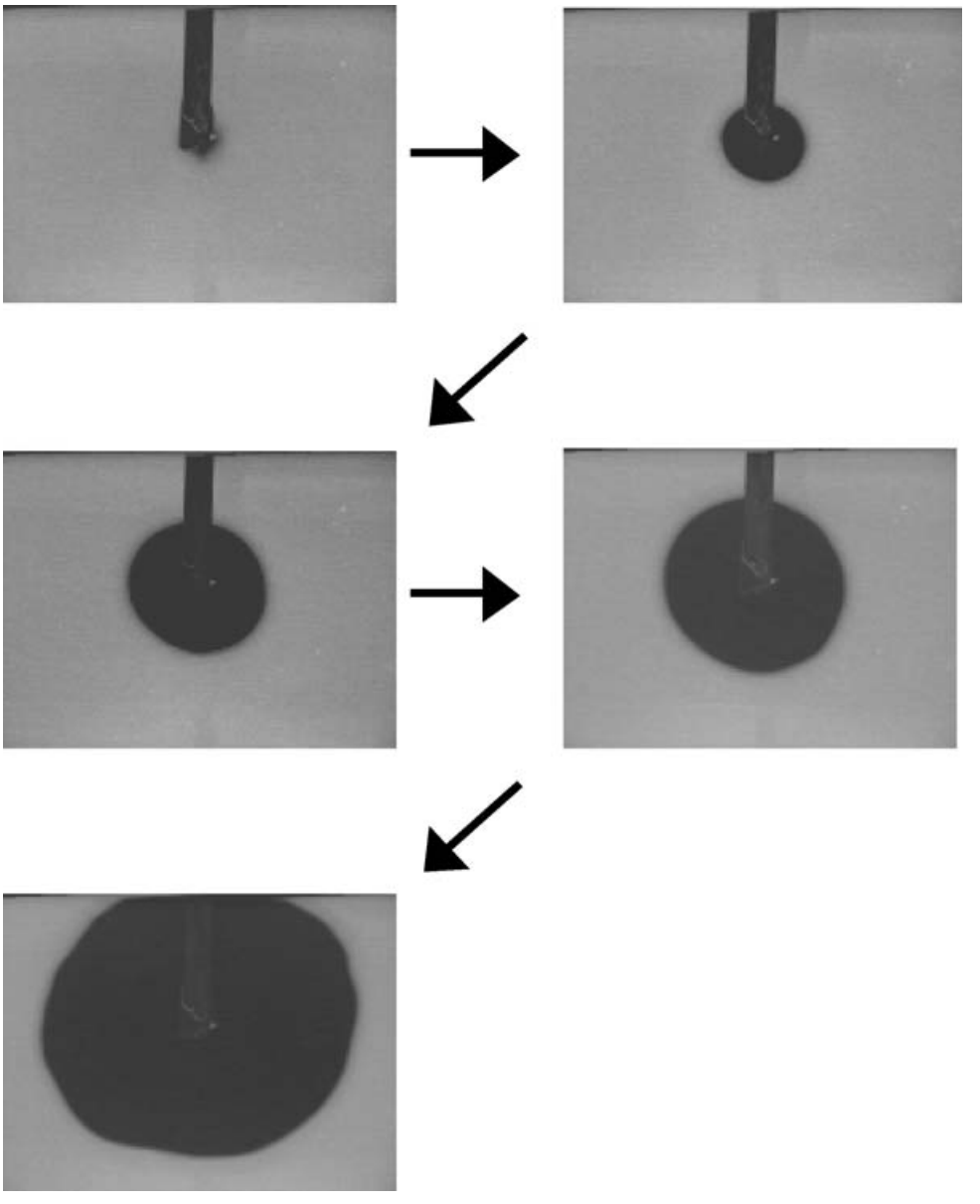

FIGURE 13. Opening of a dry spot on a thin film of fluid B. The first four images were taken at 1 s intervals with 40 s intervals between the fourth and last image which is within 1 mm of the static diameter.

opening and closing cases represent instances where the dry spot did not close after a hole was blown or did not open after having a small hole blown. The thinnest initial depth in the figure represents a limit for the experiment because the static value for the opening diameter was approaching the diameter of the containment ring.

In figure 17, the quasi-steady theory of Lopez *et al.* (2001) is plotted along with the experimental results for the initial film thickness, $H_0 = 1.9$ mm, and 2.0 mm. Here, the scaled radius (in units of $\sqrt{\sigma/\rho g}$) is plotted as a function of the scaled time (in units of the total time of observation, see figure 15). As in figure 8, the static contact

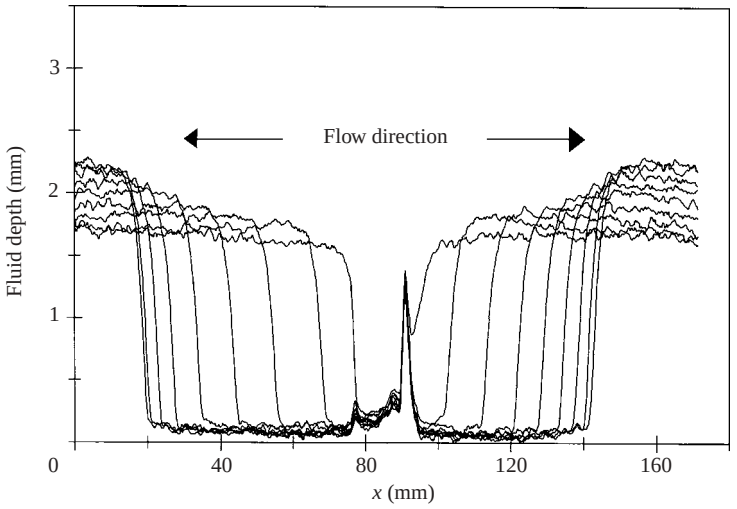

FIGURE 14. Plots as a function of time of the opening of a dry spot in a thin film of fluid B. The plots are at 1 s intervals. The spike in the fluid depth at $x = 95$ mm is because the support rod for the air hose is in view of the camera.

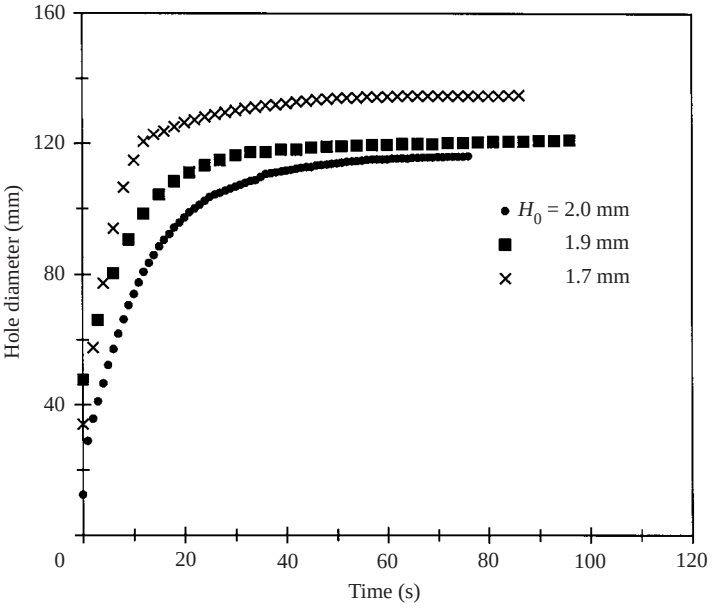

FIGURE 15. Hole diameter of an opening dry spot as a function of time for varying fluid depths. Experimental fluid is fluid B.

angle was selected so that the theory and experimental predictions were the same at the final data point. As before, this static contact angle was similar to those predicted by the theory. In this case, the selection of this contact angle was straight-forward since it is determined by the observed static hole diameter and the known volume of liquid. We see that there is reasonable agreement between the theory and experiment, but the experiment has a more rapid initial increase in hole diameter. This could be due to the fact that the quasi-steady model is being used for comparison, as opposed

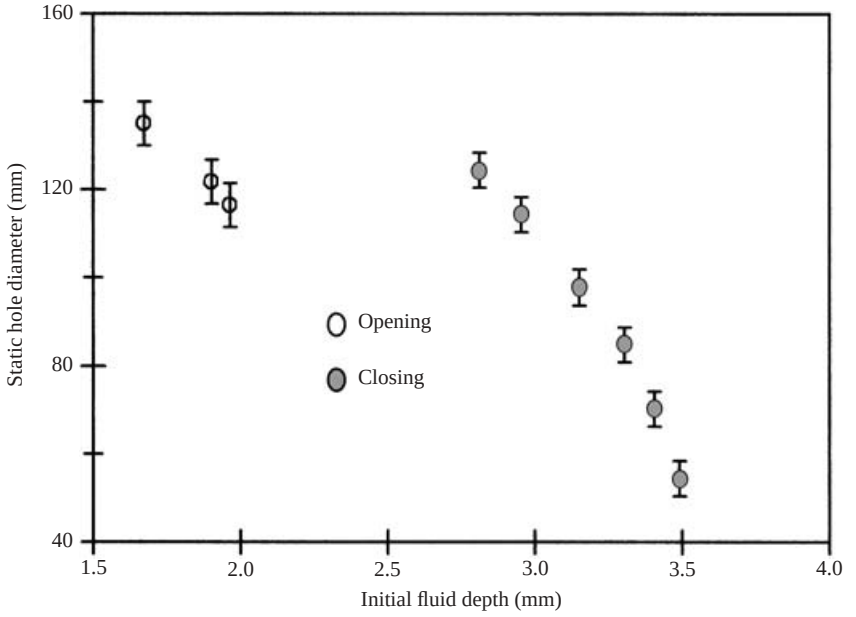

FIGURE 16. Plot of static hole diameter as a function of initial fluid depth for both an opening and closing dry spot. Experimental fluid is fluid B.

to a model which accounts properly for the time-dependent evolution of the dry spot. It could also be due to how the slip-velocity is related to the contact angle in the model (i.e. equation (3.3)).

4.4. *Fluid front speed and contact (or face) angle*

The speed of a fluid front and the contact (or face) angle for both a closing and opening hole can be determined by our experimental technique. This is one of the advantages of the fluorescent imaging method since it allows us to record the contact or face angle of the fluid front as the front moves through time. Results for a closing dry spot are given in figure 18. The data show that the dry spot initially collapses very quickly, but slows down significantly within 10 s. After 30 s the fluid front of the dry spot has come to a virtual stop and the spot is approximately at its static shape. It is interesting to compare the speed of the front with the change of the face angle as a function of time. The data show that the face angle also experiences a similar change to the speed, i.e. the face angle is decreasing initially and is approximately a constant static value within 30 s. The error of the fluorescent imaging method results in an error of the measurement of the face angle of approximately 3° (Johnson *et al.* 1997, 1999). Notice in figure 18 that the initial slight decrease in face angle corresponds to an initially steady decrease in fluid front speed. In figure 19, we present data for an opening dry spot of fluid B. Here, the face angle has reversed its trend and is increasing initially as the spot opens. In addition, we see that the front speed is initially decreasing. Our experimental results for the dynamics of the face angle are consistent with other experimental results which imply that the contact angle is a monotonically increasing function of contact line velocity (Dussan V. 1979; de Gennes 1985).

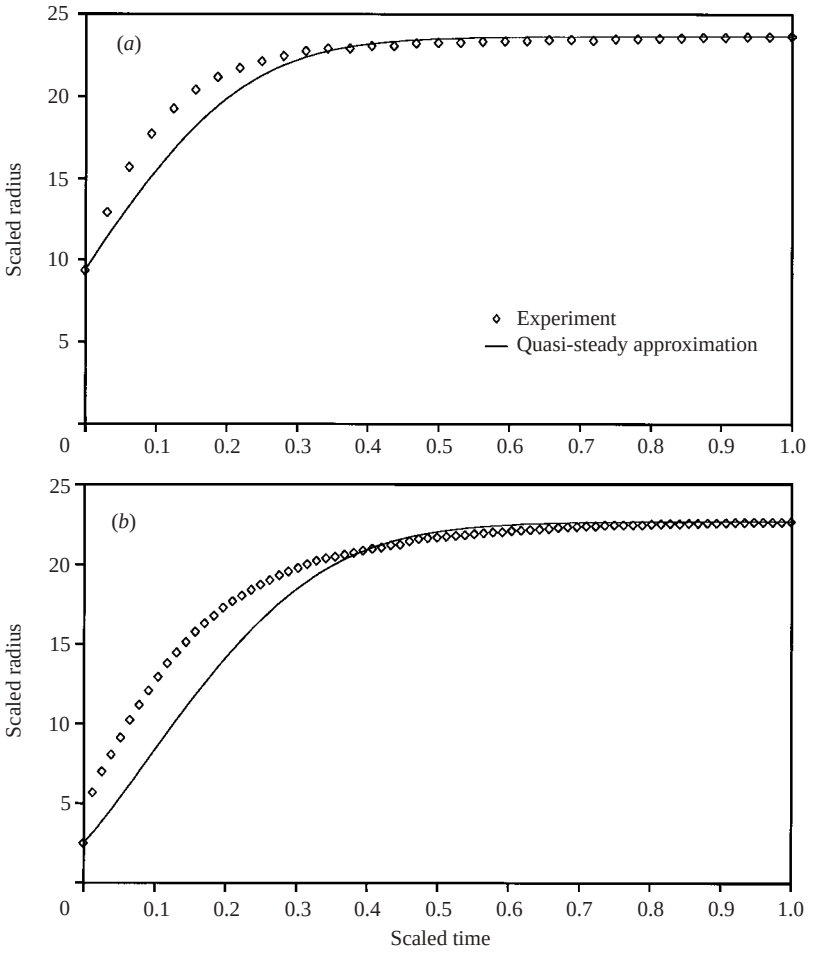

FIGURE 17. Comparison between the quasi-steady theory and experiment for a opening dry spot with initial film thickness (*a*) $H_0 = 1.9$ mm, (*b*) 2.0 mm.

4.5. *Different containment rings*

The effect of changing the diameter of the containment ring on a fully closing dry spot is shown in figure 20. Here, we consider a film with an initial thickness of 3.22 mm. The same puff of air was given to the film in each of the different rings. Hence, the initial dry spot diameter differed for each of the different diameter rings with the smaller diameter ring having the smallest initial dry spot diameter, since the effect of the ring wall is felt more easily in this case. For this thick film, the blown holes completely closed. As shown in figure 20, the larger the ring diameter, the more slowly the dry spot closed. Some variation in the static hole diameter was also observed (as much as 20% in some cases), but the overall dynamics were qualitatively similar to the results presented here.

5. Discussion

We have presented both experimental and theoretical results for the dynamics of dry spots. Three different dry spot behaviours were observed, depending on the initial

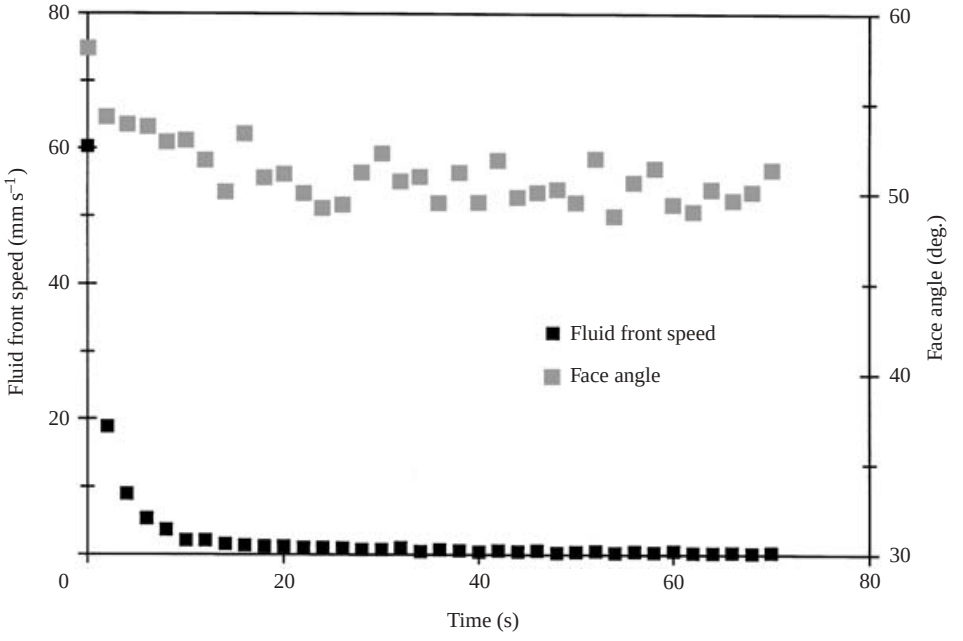

FIGURE 18. Plot of the fluid front speed and face angle as a function of time for a closing dry spot. The fluid is fluid A.

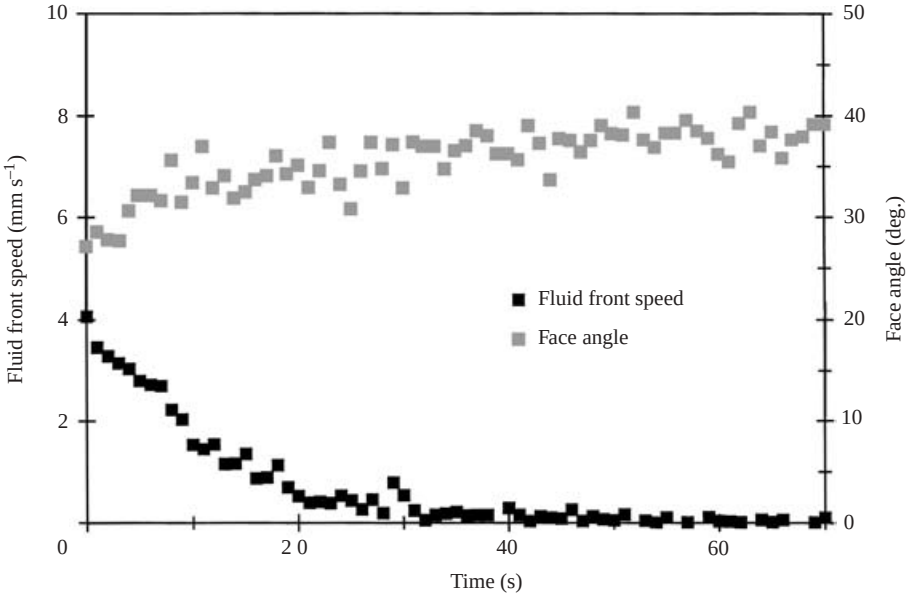

FIGURE 19. Plot of the fluid front speed and face angle as a function of time for an opening dry spot. The fluid is fluid B.

film thickness and the outer ring diameter. In particular, we found that a dry spot could completely close, it could evolve into a steady shape, or it could remain static at the blown shape. The quasi-steady model of Lopez *et al.* (2001) has been shown to describe the evolution of the dry spot reasonably well. This is true even though

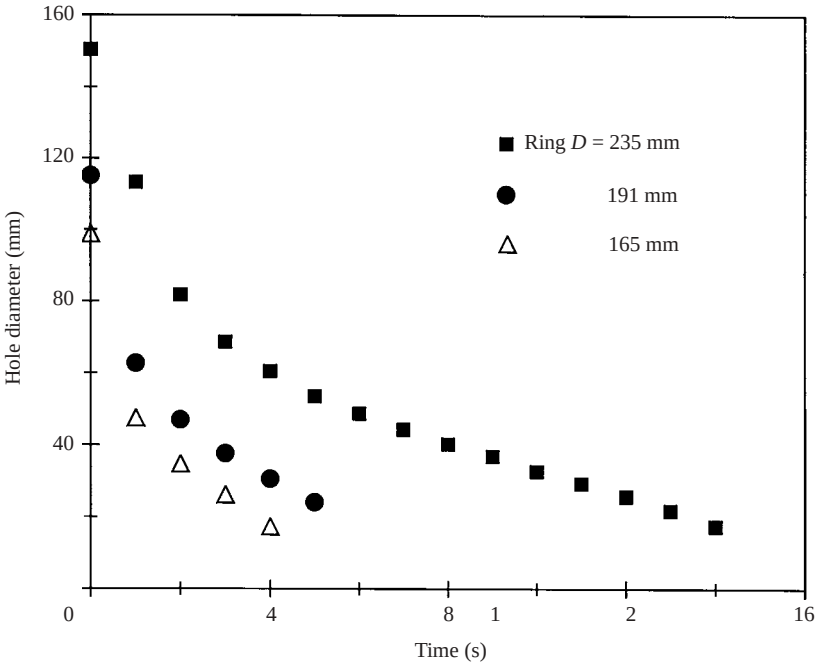

FIGURE 20. Hole diameter of a fully closing hole of fluid C as a function of time for three different containment rings.

we have in some cases used it in limits, e.g. large contact angles, where is it not expected to be applicable. However, when applicable, this is a good model to use for predictions since certain physical parameters necessary for predicting the dynamics of the dry spot and of the liquid film interface are not required to be known explicitly if we select the appropriate scales when comparing to the experimental data. For a closing dry spot, the behaviour near the collapse time compares well with the work of Diez *et al.* (1992) who neglect surface-tension effects.

This physical system is unusual, in that the attractor is one-sided. In particular, if the initial dry spot is larger than the equilibrium value, it tends to close, but if it is smaller, it does not open further, at least within the range of parameters investigated. A one-sided attractor for hole opening and closing of these films is probably related to the existence of separate advancing and receding contact angles. In between these two contact angles, these is a dead zone of angles for which the contact line is motionless. This phenomenon is known as contact angle hysteresis. Surface roughness is expected to be responsible for contact angle hysteresis. Even though care was taken in smoothing our substrate, and a silicone film was applied, hysteresis effects still appear to be of some significance. Note that because of the microscopic roughness, the advancing contact angle is generally larger than the receding contact angle. This hypothesis might be tested by using a nanometrically smooth, clean and corrosion-free solid plate to minimize contact-angle hysteresis.

This work was supported in part by NSF Grant CTS9633959. MJM was also supported in part by DOE Grant DE-FG02-88ER13927 and NSF Grant DMS-0104935.

REFERENCES

Diez, J. A., Gratton, R. & Gratton, J. 1992 Self-similar solution of the second kind for a convergent viscous gravity current. *Phys. Fluids* A **4**, 1148–1155.

Dussan, V., E. B. 1979 On the spreading of liquids on solid surfaces: static and dynamic contact lines. *Annu. Rev. Fluid Mech.* **11**, 371–400.

de Gennes, P. G. 1985 Wetting: statics and dynamics. *Rev. Mod. Phys.* **57**, 827–863.

Greenspan, H. P. 1978 On the motion of a small viscous droplet that wets a surface. *J. Fluid Mech.* **84**, 125–143.

Johnson, M. F. G. 1997 Experimental study of a thin liquid film flowing down an inclined plane. PhD thesis, Northwestern University.

Johnson, M. F. G., Schluter, R. A. & Bankoff, S. G. 1997 Fluorescent imaging system for global measurement of liquid film thickness and dynamic contact angle in free surface flows. *Rev. Sci. Instrum.* **68**, 4097–4102.

Johnson, M. F. G., Schluter, R. A., Miksis, M. J. & Bankoff, S. G. 1999 Experimental study of rivulet formation on an inclined plate by fluorescent imaging. *J. Fluid Mech.* **394**, 339–354.

Keller, J. B. & Miksis, M. J. 1983 Surface tension driven flows. *SIAM J. Appl. Maths* **43**, 268–277.

Lamb, H. 1916 *Statics*. Cambridge University Press.

Lopez, P. G., Miksis, M. J. & Bankoff, S. G. 2001 Stability and evolution of a dry spot. *Phys. Fluids* **13**, 1601–1614.

Moriarty, J. A. & Schwartz, L. W. 1993 Dynamic considerations in the closing and opening of holes in thin liquid films. *J. Colloid Interface Sci.* **161**, 335–342.

Padday, J. F. 1971 The profiles of axially symmetric menisci. *Phil. Trans. R. Soc.* **269**, 265.

Redon, C., Brochard Wyart, F. & Rondelez, F. 1991 Dynamics of dewetting. *Phys. Rec. Lett.* **66**, 715–718.

Sharma, A. & Ruckenstein, E. 1990 Energetic criteria for the breakup of liquid films on nonwetting solid surfaces. *J. Colloid Interface Sci.* **137**, 433–445.

Taylor, G. I. & Michael, D. H. 1973 On making holes in a sheet of fluid. *J. Fluid Mech.* **58**, 625–641.

Wilson, S. K. & Duffy, B. R. 1996 An asymptotic analysis of small holes in thin fluid layers. *J. Engng Maths* **30**, 445–457.